Rev7 and 53BP1/Crb2 prevent RecQ helicase-dependent hyper-resection of DNA double-strand breaks

Bryan A. Leland, Angela B. Chen, Amy Y. Zhao, Robert C. Wharton, and Megan C. King

Department of Cell Biology, Yale School of Medicine, New Haven, CT 06520

Correspondence to megan.king@yale.edu

Abstract

Poly(ADP ribose) polymerase inhibitors (PARPi) target cancer cells deficient in homology-directed repair of DNA double-strand breaks (DSBs). In preclinical models, PARPi resistance is tied to altered nucleolytic processing (resection) at the 5' ends of a DSB. For example, loss of 53BP1 or Rev7/MAD2L2/FANCV derepresses resection to drive PARPi resistance, although the mechanisms are poorly understood. Long-range resection can be catalyzed by two machineries: the exonuclease Exo1, or the combination of a RecQ helicase and Dna2. Here, we develop a single cell assay that allows the distinct phases and machineries of resection to be interrogated simultaneously in living *S. pombe* cells. Using this assay, we find that the 53BP1 orthologue and Rev7 specifically repress long-range resection through the RecQ helicase-dependent pathway, thereby preventing hyper-resection. These results suggest that "rewiring" of BRCA1-deficient cells to employ an Exo1-independent hyper-resection pathway is a driver of PARPi resistance.

Introduction

DNA repair is an essential process conserved throughout evolution and commonly disrupted in tumor cells (Jeggo et al., 2016). Many cancer treatments, including poly(ADP ribose) polymerase (PARP) inhibitors (PARPi), target DNA repair pathways to kill rapidly dividing, repair-deficient cells (Farmer et al., 2005; Fojo and Bates, 2013; Lord et al., 2015; Mateo et al., 2015). 5' end resection, which generates tracts of single-strand DNA (ssDNA) at DNA double-strand break (DSB) ends dictates repair pathway choice: blocking resection promotes canonical non-homologous end joining (typically in G1), while initiating resection commits a DSB to repair by homologous recombination (HR), usually in S/G2 (Chapman et al., 2012; Hustedt and Durocher, 2016; Symington, 2016). The resection machinery is tightly controlled at both the step of resection initiation (involving Ctp1/Sae2/CtIP and the MRN/X complex) and during long-range resection, which is mediated by two parallel pathways catalyzed by either the exonuclease Exo1 or the combination of a RecQ helicase and Dna2 (Chen et al., 2012; Croteau et al., 2014; Nimonkar et al., 2011; Tkáč et al., 2016; Zimmermann et al., 2013). Additional accessory factors play key roles as modulators of resection; for example, loss of Rev7/MAD2L2/FANCV, a small, multifunctional HORMA domain protein, (Bluteau et al., 2016; Rosenberg and Corbett, 2015) derepresses resection inhibition (Boersma et al., 2015; Xu et al., 2015), thereby allowing HR-deficient, *Brca1*$^{-/-}$ *p53*$^{-/-}$ cells to become resistant to PARPi. In human cells, Rev7 appears to act in concert with another inhibitor of resection, 53BP1(Chapman et al., 2013; Ochs et al., 2016; Zimmermann et al., 2013), loss of which is also sufficient to drive PARPi resistance (Boersma et al., 2015; Bouwman et al., 2010; Jaspers et al., 2013; Xu et al., 2015). Importantly, the mechanisms by which Rev7 and 53BP1 inhibit DSB end resection remain poorly understood. To gain insights into how resection is controlled, we have developed a single-cell microscopy-based assay capable of quantitatively measuring DSB end resection rates in the facile genetic model, *S. pombe*. Leveraging this assay, we find that Rev7 and the 53BP1 orthologue, Crb2, specifically inhibit the RecQ-helicase-dependent long-range resection pathway. Moreover, through derepression of RecQ helicases, *rev7*Δ or *crb2*Δ cells can achieve very fast resection rates (>20 kb/hr) – approximately twice as fast as Exo1-dependent long-range resection. As BRCA1 activity has been tied to Exo1-dependent long-range resection (Tomimatsu et al., 2012), our findings suggest that PARPi resistance can be driven by compensation through derepression of the RecQ-helicase-dependent resection pathway.

Results

A microscopy-based assay to measure resection rates in single cells

In order to quantitatively measure initial steps in DSB processing in single, living cells, we developed a microscopy-based DSB end resection assay (Figure 1A). In this system, an ectopic 10.3 kb, 256-copy LacO array and adjacent HO endonuclease cut site are engineered at a euchromatic (but intergenic) region near *Mmf1* (Figure 1–figure

supplement 1). A single, site-specific DSB is generated by regulating the expression of the HO endonuclease under the control of the Ura-inducible $P_{urg1lox}$ RMCE system (Watson et al., 2008; 2011). The timing of on-target DSB events is visualized by the appearance of a Rad52(Rad22)-mCherry focus that co-localizes with Mmf1:LacO/LacI-GFP (Figure 1B). As resection proceeds the LacO repeats become single stranded, disupting LacI-GFP binding and causing the intensity of the GFP focus to progressively decrease (Bell and Lewis, 2001) (Figure 1A,B, Figure 1–figure supplement 2). By tracking cell lineages, we see that HO endonuclease induction produces on-target Rad52-mCherry foci in S/G2 (G1 is very short in *S. pombe*) when the repair machinery is primed for HR (Symington and Gautier, 2011) (Figure 1B). Importantly, we do not observe loading of Rad52-mCherry at the LacO/LacI-GFP array in the absence of HO endonuclease expression (on-target Rad52 foci in < 0.2% of uninduced cells, n=657), suggesting that the LacO array is not sufficient to create a "fragile site" in *S. pombe* (Jacome and Fernandez-Capetillo, 2011; Saad et al., 2014).

This assay only visualizes DSB foci after resection initiation by Ctp1/Sae2/CtIP and MRN/MRX (~100 nt of resection), as Rad52 loads at DSBs by exchanging with RPA on resected ssDNA ends (Jensen and Russell, 2016; Lisby et al., 2004; Ma et al., 2015; Mimitou and Symington, 2008). Using quantitative imaging with calibration strains, we estimate that visualization of the Rad52-mCherry focus requires loading of ~30 copies (see Methods), representing a Rad52 filament equivalent to at least 90 nt (but likely several hundred nts, see below) of resected ssDNA on each sister in G2 (Gibb et al., 2014; Grimme et al., 2010; Kagawa et al., 2002; Singleton et al., 2002; Swartz et al., 2014; Wu and Pollard, 2005). To test the frequency with which resection initiation leads to visible Rad52 foci in this assay, we compared the timing of Rad52-mCherry foci formation to an independent measure of resection using a quantitative PCR (qPCR) assay in which resection protects from digestion at an ApoI cut site 168 nt downstream of the HO cut site (Langerak et al., 2011) (Figure 1–figure supplement 3A). Using this qPCR based assay, we observe similar kinetics for ApoI protection and Rad52 focus formation, with an apparent 30-60 minute delay between ApoI protection (qPCR) and Rad52-mCherry loading, which likely represents the time required for RPA loading and exchange to form the nucleoprotein filament (Lisby et al., 2004) (Figure 1–figure supplement 3B). We observe an on-target DSB level of ~15% per S phase.

To confirm that the decrease in LacI-GFP focus intensity results from long-range resection, we analyzed cells lacking Exo1. Exo1 catalyzes the majority of long-range resection in WT *S. pombe*, with the Rqh1/Sgs1/BLM and Dna2 resection pathway playing a secondary role (Langerak et al., 2011). Indeed, we detect a strong inhibition of resection (comparable to *ctp1*Δ cells) as close as 300 nts from the DSB in cells lacking Exo1 as detected by qPCR (Figure 1–figure supplement 3C); this correlates with a major defect in Rad52-mCherry loading in the imaging-based resection assay (Figure 1–figure supplement 3D). This observation confirms that the extent of resection required to form visible Rad52 foci in this assay (~30 molecules; ≥ 300 nt) partially requires

Exo1-dependent resection in addition to MRN/MRX- and Ctp1/Sae2/CtIP-dependent resection initiation (Symington, 2016).

By measuring the time interval between Rad52-mCherry focus formation (again, ≥300 bp of resection; Figure 1–figure supplement 3B-C) and LacO/LacI-GFP focus disappearance (estimated to occur when <500 bp of the LacO array remains unresected) (Figure 1–figure supplement 3E), we calculate a median, long-range resection rate of 7.6 kb/hr in WT cells (Figure 1C). This rate is somewhat faster than the mean resection rates measured by previous population-based assays using qPCR in *S. pombe* (4 kb/hr) or Southern blot in *S. cerevisiae* (4.4 kb/hr) (Langerak et al., 2011; Zhu et al., 2008). The somewhat faster rate determined here could be because this assay isolates the process of long-range resection after Rad52 loading. Importantly, using the qPCR approach to compare resection upstream of the DSB (which contains the LacO array) and downstream of the DSB (which does not) demonstrates that any influence of the LacO array on resection rate is minor (Figure 1D). As expected, resection in the absence of Exo1 is very slow (Figure 1E); LacO disappearance takes longer than 5 hours – the limit of data acquisition due to photobleaching; from this we infer an upper bound of ~2.8 kb/hr for the resection rate in *exo1*Δ cells.

53BP1 (in human cells) and its orthologue Rad9 (in budding yeast) repress resection initiation (Chapman et al., 2012; Ferrari et al., 2015; Symington, 2016); in budding yeast, loss of Rad9 also increases resection efficiency (Bonetti et al., 2015). Applying the live cell resection assay to fission yeast lacking the orthologous Crb2, we observe a strong increases the median rate of resection to (13.9 kb/hr), with some individual cells demonstrating very fast (~40 kb/hr) resection rates (Figure 1C). Thus, we can readily assess factors that positively and negatively influence long-range resection rate using this approach.

Rev7 inhibits long-range resection

Next, we examined how loss of Rev7 influences long-range resection at DSBs during S/G2. Consistent with previous studies, and similar to Crb2, we find that Rev7 inhibits long-range resection, with a median resection rate of 10.4 kb/hr in *rev7*Δ cells (Figure 2A,B). As Rev7 also functions with Rev3 as part of the polymerase ζ complex in translesion synthesis, we also confirmed that Rev3 does not affect resection (Figure 2B), consistent with previous data showing that repressing resection during HR is a distinct function of Rev7 (Boersma et al., 2015; Rosenberg and Corbett, 2015; Xu et al., 2015). Using the orthogonal qPCR approach (Figure 1–figure supplement 3A), we confirm that in *rev7*Δ cells, more chromosomes with DSBs have undergone 13kb of resection (Figure 2C). Thus, loss of Rev7 increases the rate of long-range resection to an extent similar to that seen in cells lacking Crb2.

The RecQ helicase, Rqh1, rather than Exo1, drives hyper-resection in the absence of Crb2 and Rev7

We next asked if Crb2/Rad9/53BP1 and Rev7/MAD2L2 inhibit long-range resection through the Exo1 pathway, the RecQ helicase (Rqh1)-Dna2 pathway, or both (Symington and Gautier, 2011). Interestingly, we find that the rapid long-range resection rate observed in *crb2*Δ or *rev7*Δ cells is entirely Exo1-independent (Figure 3A-C, Figure 3–figure supplement 1). In stark contrast, the rapid rate of resection in a *rev7*Δ single mutant is entirely dependent on the presence of Rqh1 (Figure 3A). Consistent with these observations, we find that loss of Rev7 is able to rescue the severe growth defect of *exo1*Δ cells on rich media plates containing camptothecin, consistent with a derepression of Rqh1-dependent resection in the absence of a functional Exo1 pathway (Figure 3D). When considering only precisely determined resection events, the average long-range resection rate in *crb2*Δ cells is not statically less than that of *crb2*Δ*rqh1*Δ cells when correcting for multiple comparisons ($p = 0.16$) (Figure 3A). However, in many *crb2*Δ*rqh1*Δ cells, resection durations extend beyond the timeframe of data acquisition, suggesting that rapid *crb2*Δ resection also requires Rqh1 (Figure 3–figure supplement 2).

Taken together, these results strongly suggest that loss of either Rev7 or Crb2 drives a shift in resection pathway mechanism from Exo1 to the RecQ helicase-dependent pathway. Unlike Exo1-driven resection that dominates in WT cells, *crb2*Δ or *rev7*Δ cells in which the RecQ helicase is derepressed are capable of resection rates in excess of 20 kb/hr, indicating that the RecQ helicases are more capable of to drive hyper-resection of DSBs than the Exo1-dependent pathway. The strong inhibition of RecQ helicase-dependent resection by Crb2 and Rev7 also explains why Rqh1 is not a major player in WT *S. pombe* resection, since Rqh1 can be derepressed to such a large extent (by loss of Crb2 or Rev7) that Exo1 becomes dispensable for long-range resection in *crb2*Δ*exo1*Δ and *rev7*Δ*exo1*Δ cells (Figure 3A).

Rev7 and Crb2 have distinct roles early in resection

The LacO-based resection assay was designed primarily to measure the rate of long-range resection in single cells by timing the duration between Rad52 foci formation and LacO/LacI-GFP focus disappearance. However, we also observe the frequency and timing of Rad52 focus formation events across the population of cells, giving us some insight into early resection events: initiation by Ctp1/Sae2/CtIP and MRN/MRX followed by enough Exo1/Rqh1-dependent long-range resection (>300bp) for binding of Rad52-mCherry to form a visible focus (Figure 1–figure supplement 3). Cells lacking Crb2 form detectable Rad52 foci at WT levels and with similar kinetics (Figure 4A,B, Figure 4–figure supplement 1). This observation contrasts with studies of the orthologous Rad9 and 53BP1, which are thought to inhibit both resection initiation by Ctp1/Sae2/CtIP as well as long-range resection (Chapman et al., 2012; Ferrari et al., 2015; Symington, 2016). We suspect that this observation reflects that Crb2/Rad9/53BP1 primarily act as inhibitors of Ctp1- and/or MRN/X-dependent resection initiation in G1, while in this fission yeast assay all DSBs are formed in S/G2 (Figure 1A,B) (Branzei and Foiani, 2008; Chapman et al., 2012). Importantly, loss of Crb2 is able to rescue the Rad52 loading defect in an *exo1*Δ background, confirming that inefficient resection initiation

and/or short-range resection in cells lacking Exo1 can be overcome in the absence of Crb2 (Figure 4A,B, Figure 4–figure supplement 1).

Given that Crb2 and Rev7 both act as inhibitors of long-range resection, we were surprised to observe a large reduction in the percentage of cell cycles with on-target Rad52 foci formation in *rev7*Δ cells (Figure 4A,B). This effect is almost as striking as in *exo1*Δ cells, but is not seen in cells lacking Rev3, again suggesting that Rev7 is acting independently from its role in translesion synthesis (Figure 4A). Consistent with this, the timing of Rad52 loading after HO endonuclease induction is delayed in *rev7*Δ cells, similar to *exo1*Δ cells (Figure 4B, Figure 4–figure supplement 1). To test if Rev7 might negatively influence Rad52 loading rather than early steps in resection, we again employed an orthogonal qPCR approach (Figure 1–figure supplement 3A). Consistent with our interpretation that the delay in Rad52-mCherry loading in the absence of Rev7 reflects slower generation of the first few hundred nts of resected DNA, population measurements by qPCR indicate slightly less efficient resection near to the DSB (~300 nts; Figure 4C; importantly, at this phase the extent of resection through 300 bps is still rising, compare to Figure 1–figure supplement 3B). This stands in contrast to a clear gain in resection efficiency in *rev7*Δ cells assessed far from the DSB (~3 kb), consistent with the increased rate of long-range resection in cells lacking Rev7 (Figure 2). Thus, although the population-based qPCR assay hints that Rev7 influences short- and long-range resection differently, the single-cell assay we have developed is able to cleanly reveal long-range resection rates independent from delays in initiation, highlighting the utility of this approach in future work. Further support for this interpretation comes from the observation that cells lacking Rev7 show delayed Rad52 loading relative to the previous mitosis (Figure 4D), and increased cell length at the time of Rad52 focus formation, indicating a more prolonged checkpoint activation from the time of DSB formation (Figure 4E).

Consistent with differential effects of Crb2 and Rev7 during resection initiation, while loss of Crb2 can overcome the need for Exo1 to form Rad52 foci, loss of Rev7 cannot (Figure 4A,B). In rare cases, *rev7*Δ*exo1*Δ cells have static, very low levels of Rad52 association with the DSB persisting for > 2 hrs before progressive, rapid long-range resection through the LacO array, again consistent with a stall in early resection, followed by rapid, progressive, long-range resection (Figure 4F). Interestingly, loss of Rqh1 in the *rev7*Δ background is able to reconstitute normal rates of resection initiation (Figure 4A,B); the origin of this effect is not yet clear, and will require further study. Importantly, as in *exo1*Δ cells, loss of Crb2 can suppress the early resection defect in *rev7*Δ cells, restoring both the frequency and timing of Rad52 focus formation (Figure 3A,B). Thus, while Crb2 inhibits early resection, similar to 53BP1/Rad9, these data suggest a distinct role for Rev7 at an early phase of resection.

Discussion

Using a microscopy-based assay capable of quantitatively measuring DSB end resection in living cells, we show that Crb2/Rad9/53BP1 and Rev7/MAD2L2 act as specific inhibitors of RecQ helicase-mediated long-range resection (Figure 2). This result is consistent with the observation that specific mutations in the budding yeast RecQ helicase, Sgs1, can disrupt inhibition by the Crb2 orthologue, Rad9, leading to a gain in Sgs1-dependent resection (Bonetti et al., 2015). By analyzing single-cell data, we also find evidence for a distinct role for Rev7 early in resection, with both Rev7 and Exo1 required for the normal frequency and kinetics of Rad52 focus formation (Figure 4). This contrasts with inhibition of resection initiation by Crb2/Rad9/53BP1, although we find that loss of Crb2 is able to rescue the early resection defect in both *rev7*Δ or *exo1*Δ cells (Figure 4).

Importantly, loss of either 53BP1 or Rev7 allows *BRCA1*$^{-/-}$ *p53*$^{-/-}$ cells to become resistant to PARP inhibitors (Jaspers et al., 2013; Xu et al., 2015). As BRCA1-deficient cells have compromised CtIP- and Exo1-dependent resection, it was previously suggested that loss of 53BP1 or Rev7 could restore HR, thereby overcoming the increased DSB load caused by PARP inhibitors (Polato et al., 2014; Tomimatsu et al., 2012). This study reveals that not just the efficiency, but also the molecular mechanism of resection is altered upon loss of Crb2/53BP1 or Rev7. We expect these insights to have several consequences. First, RecQ helicases, when paired with Dna2, are capable of exceptionally fast resection *in vitro* (Niu et al., 2010), which when derepressed by loss of 53BP1 or Rev7 could cause extended tracts of ssDNA several kb long, promoting further genome instability (Hicks et al., 2010; Ochs et al., 2016); indeed, our data point to such a hyper-resection phenotype upon loss of either Crb2 or Rev7 (Figure 2B). Second, our results suggest that inhibitors of RecQ helicases could potentially re-sensitize BRCA1-null cells to PARP inhibitors, since this would make them both Exo1- and RecQ helicase-deficient (Aggarwal et al., 2013; Yazinski et al., 2017).

Materials and Methods:

Cell culture, strain construction and verification

The strains used in this study are listed in Supplementary file 1. *S. pombe* were grown, maintained, and crossed using standard procedures and media (Moreno et al., 1991). Gene replacements were made by exchanging open reading frames with various MX6-based drug resistance genes (Bähler et al., 1998; Hentges et al., 2005). The 10.3 kb LacO array was inserted between *Mmf1* and *Apl1* on the right arm of chromosome II (Chr II: 3,442,981) using a modified two-step integration procedure that first creates a site-specific DSB to increase targeting efficiency of linearized plasmid pSR10_ura4_10.3kb (Leland and King, 2014; Rohner et al., 2008). A modified MX6-based hygromycin-resistance cassette containing the HO cut site was then inserted between *Apl1* and *Mug178* on chromosome II (Chr II: 3,446,249), 3.2 kb distal to the LacO insertion. The total distance between the HO cut site and the beginning of the 10.3 kb LacO array is 3.57 kb. As the LacO array can contract during the process of transformation, integrants were screened by HincII digest followed by Southern blot (Figure 1–figure supplement 1) using standard procedures, a biotin-conjugated LacO probe, and a Streptavidin-HRP chemilluminescent detection system (Thermo #N100 & #34096).

DSB induction using $P_{urg1lox}$-HO

We used the uracil-responsive $P_{urg1lox}$ expression system, with slight modifications, to induce HO endonuclease expression and create site-specific DSBs at the HO cut site (Watson et al., 2011; Watt et al., 2008). We performed a fresh integration of the *HO* gene at the endogenous *urg1* locus for each experiment in order to reduce long-term instability at the HO cut site or the development of HO resistance presumably due to insertion/deletion events caused by basal expression levels of HO. The pAW8E*Nde*I-HO plasmid (a gift from Tony Carr) was transformed into *S. pombe*, which were then plated onto EMM-leu+thi-ura plates (-leucine: plasmid selection; +thiamine: P_{nmt1}-*Cre* repression; -uracil: $P_{urg1lox}$-*HO* repression). After 4-5 days of growth at 30°C, 40-100 individual colonies were combined to obtain a reproducible plasmid copy number across the population. Cre-mediate *HO* gene exchange at the endogenous Urg1 locus (*urg1::RMCE*$_{bleMX6}$) was induced by overnight culture in EMM-thi-ura+ade+NPG media (-thiamine: expression of Cre from pAW8E*Nde*I-HO; -uracil: $P_{urg1lox}$-*HO* repression; +0.25mg/mL adenine: reduce autofluorescence; +0.1mM n-Propyl Gallate (NPG): reduce photobleaching in microscopy experiments, prepared fresh). The following day, site-specific DSBs were induced in log-phase cultures by the addition of 0.50 mg/ml uracil. This induction strategy resulted in ~15% of cells making a DSB within ~2 hrs (Figure 1C).

qPCR resection assay

Initiation of resection was assessed using a previously described qPCR assay where ssDNA produced by resection causes protection from ApoI digestion (Langerak et al., 2011). ApoI cut site positions (relative to the HO cut cite (Chr II: 3446192)) and PCR primer sets spanning each ApoI recognition site can be found in Supplementary file S3. Mock HincII digestions (do not affect qPCR products) and additional control primers at Ncb2 were used to normalize for ApoI digestion efficiency (see Supplementary Table S3).

Microscopy

All images were acquired on a DeltaVision widefield microscope (Applied Precision/GE) using a 1.2 NA 100x objective (Olympus), solid-state illumination, and an Evolve 512 EMCCD camera (Photometrics). Slides were prepared ~20 minutes after adding 0.50 mg/ml uracil to log-phase cultures to induce HO endonuclease expression and DSB formation. Cells were mounted on 1.2% agar pads (EMM +0.50 mg/ml uracil, +2.5 mg/ml adenine, +0.1 mM freshly prepared NPG) and sealed with VALAP (1:1:1 vaseline:lanolin:paraffin). Image acquisition began between 40 and 80 minutes after uracil addition. Imaging parameters for all resection assay data acquisition were as follows. Transmitted light: 35% transmittance, 0.015 sec exposure; mCherry: 32% power, 0.08 sec exposure; GFP: 10% power, 0.05 sec exposure. At each time point (every 10 min for 5-7 hrs), 25 Z-sections were acquired at 0.26 μm spacing. Identical imaging parameters were used to image a strain expressing endogenously tagged Sad1-mCherry (Sad1 forms a single focus at the spindle pole body that contains between 450 and 1,030 molecules) and relative mCherry foci intensities were used to determine that ~30 molecules of Rad52-mCherry are required to detect a visible focus with these imaging parameters (Wu and Pollard, 2005).

Image analysis

For the LacO resection assay, every cell cycle was quantified individually, including timing of nuclear division, cellular division, Rad52-mCherry focus formation, and LacO/LacI-GFP focus disappearance. Only on-target Rad52 foci (that co-localized with LacO/LacI-GFP for at least 2 frames) were considered, since many DSB events occur spontaneously, especially during S-phase. The number of cells and events used to generate the plots in all Figures is included as Supplementary file 2. The time between the first frame with an on-target Rad52-mCherry focus and the first frame with complete disappearance of the LacO/LacI-GFP focus is the duration of resection through 3.57 nt (between the HO cut site and the start of the LacO repeats) plus the full 10.3 nt LacO array. All fields from all genotypes were randomized and blinded before analysis using custom ImageJ macros. Each blinded field was first assessed for photobleaching of the LacO/LacI-GFP foci in cells without induced DSBs (>80% of all cells) to ensure that disappearance of any LacO/LacI-GFP foci in cells with on-target DSBs was due to

resection through the LacO array rather than photobleaching of the GFP signal. Raw data were processed, visualized, and analyzed using R, in particular packages dplyr, ggplot2, and broom.

Growth assays

Cells were grown overnight in YE5S media. Concentrations for each culture were monitored by both OD_{600} and a Coulter Principle cell counter (Orflow Moxi Z). Cultures were diluted as needed to ensure identical numbers of cells were spotted for each genotype, starting with ~$4x10^6$ cell/mL and going down by 6-fold dilutions. Plates were prepared using standard procedures (Moreno et al., 1991), with the addition of 30μM camptothecin (Sigma; ≥95% HPLC purified) after autoclaving.

Acknowledgements

We would thank the Susan Gasser, Tony Carr, Paul Russell, Li-Lin Du, Masayuki Yamamoto, and Julia Cooper for strains and plasmids; Jessica Johnston for generating and imaging the 1 kb LacO array strain; and Topher Carroll and Tom Pollard for helpful input and feedback. This work was supported by a National Science Foundation Graduate Research Fellowship (DGE-1122492), NIH training grant T32-HD-007180-40, and a Gruber Science Fellowship to B.A.L.; and the Searle Scholars Program and the National Institutes of Health Office of the Director (DP2OD008429-01) to M.C.K.

References

Aggarwal, M., Banerjee, T., Sommers, J.A., Iannascoli, C., Pichierri, P., Shoemaker, R.H., and Brosh, R.M. (2013). Werner syndrome helicase has a critical role in DNA damage responses in the absence of a functional fanconi anemia pathway. Cancer Res *73*, 5497–5507.

Bähler, J., Wu, J.Q., Longtine, M.S., Shah, N.G., McKenzie, A., Steever, A.B., Wach, A., Philippsen, P., and Pringle, J.R. (1998). Heterologous modules for efficient and versatile PCR-based gene targeting in Schizosaccharomyces pombe. Yeast *14*, 943–951.

Bell, C.E., and Lewis, M. (2001). The Lac repressor: a second generation of structural and functional studies. Curr. Opin. Struct. Biol. *11*, 19–25.

Bluteau, D., Masliah-Planchon, J., Clairmont, C., Rousseau, A., Ceccaldi, R., Dubois d'Enghien, C., Bluteau, O., Cuccuini, W., Gachet, S., Peffault de Latour, R., et al. (2016). Biallelic inactivation of REV7 is associated with Fanconi anemia. J. Clin. Invest. *126*, 3580–3584.

Boersma, V., Moatti, N., Segura-Bayona, S., Peuscher, M.H., van der Torre, J., Wevers, B.A., Orthwein, A., Durocher, D., and Jacobs, J.J.L. (2015). MAD2L2 controls DNA repair at telomeres and DNA breaks by inhibiting 5' end resection. Nature *521*, 537–540.

Bonetti, D., Villa, M., Gobbini, E., Cassani, C., Tedeschi, G., and Longhese, M.P. (2015). Escape of Sgs1 from Rad9 inhibition reduces the requirement for Sae2 and functional MRX in DNA end resection. EMBO Rep. *16*, 351–361.

Bouwman, P., Aly, A., Escandell, J.M., Pieterse, M., Bartkova, J., van der Gulden, H., Hiddingh, S., Thanasoula, M., Kulkarni, A., Yang, Q., et al. (2010). 53BP1 loss rescues BRCA1 deficiency and is associated with triple-negative and BRCA-mutated breast cancers. Nat Struct Mol Biol *17*, 688–695.

Branzei, D., and Foiani, M. (2008). Regulation of DNA repair throughout the cell cycle. Nat Rev Mol Cell Biol *9*, 297–308.

Chapman, J.R., Barral, P., Vannier, J.-B., Borel, V., Steger, M., Tomas-Loba, A., Sartori, A.A., Adams, I.R., Batista, F.D., and Boulton, S.J. (2013). RIF1 is essential for 53BP1-dependent nonhomologous end joining and suppression of DNA double-strand break resection. Mol Cell *49*, 858–871.

Chapman, J.R., Taylor, M.R.G., and Boulton, S.J. (2012). Playing the End Game: DNA Double-Strand Break Repair Pathway Choice. Mol Cell *47*, 497–510.

Chen, X., Cui, D., Papusha, A., Zhang, X., Chu, C.-D., Tang, J., Chen, K., Pan, X., and Ira, G. (2012). The Fun30 nucleosome remodeller promotes resection of DNA double-strand break ends. *489*, 576–580.

Croteau, D.L., Popuri, V., Opresko, P.L., and Bohr, V.A. (2014). Human RecQ helicases in DNA repair, recombination, and replication. Annu. Rev. Biochem. *83*, 519–552.

Farmer, H., McCabe, N., Lord, C.J., Tutt, A.N.J., Johnson, D.A., Richardson, T.B., Santarosa, M., Dillon, K.J., Hickson, I., Knights, C., et al. (2005). Targeting the DNA repair defect in BRCA mutant cells as a therapeutic strategy. Nature *434*, 917–921.

Ferrari, M., Dibitetto, D., De Gregorio, G., Eapen, V.V., Rawal, C.C., Lazzaro, F., Tsabar, M., Marini, F., Haber, J.E., and Pellicioli, A. (2015). Functional interplay between the 53BP1-ortholog Rad9 and the Mre11 complex regulates resection, end-tethering and repair of a double-strand break. PLoS Genet *11*, e1004928.

Fojo, T., and Bates, S. (2013). Mechanisms of resistance to PARP inhibitors--three and counting. Cancer Discov *3*, 20–23.

Gibb, B., Ye, L.F., Kwon, Y., Niu, H., Sung, P., and Greene, E.C. (2014). Protein dynamics during presynaptic-complex assembly on individual single-stranded DNA molecules. Nat Struct Mol Biol *21*, 893–900.

Grimme, J.M., Honda, M., Wright, R., Okuno, Y., Rothenberg, E., Mazin, A.V., Ha, T., and Spies, M. (2010). Human Rad52 binds and wraps single-stranded DNA and mediates annealing via two hRad52-ssDNA complexes. Nucleic Acids Res *38*, 2917–2930.

Hentges, P., Van Driessche, B., Tafforeau, L., Vandenhaute, J., and Carr, A.M. (2005). Three novel antibiotic marker cassettes for gene disruption and marker switching in Schizosaccharomyces pombe. Yeast *22*, 1013–1019.

Hicks, W.M., Kim, M., and Haber, J.E. (2010). Increased mutagenesis and unique mutation signature associated with mitotic gene conversion. Science *329*, 82–85.

Hustedt, N., and Durocher, D. (2016). The control of DNA repair by the cell cycle. Nat Cell Biol *19*, 1–9.

Jacome, A., and Fernandez-Capetillo, O. (2011). Lac operator repeats generate a traceable fragile site in mammalian cells. EMBO Rep. *12*, 1032–1038.

Jaspers, J.E., Kersbergen, A., Boon, U., Sol, W., van Deemter, L., Zander, S.A., Drost, R., Wientjens, E., Ji, J., Aly, A., et al. (2013). Loss of 53BP1 causes PARP inhibitor resistance in Brca1-mutated mouse mammary tumors. Cancer Discov *3*, 68–81.

Jeggo, P.A., Pearl, L.H., and Carr, A.M. (2016). DNA repair, genome stability and cancer: a historical perspective. Nat. Rev. Cancer *16*, 35–42.

Jensen, K.L., and Russell, P. (2016). Ctp1-dependent clipping and resection of DNA double-strand breaks by Mre11 endonuclease complex are not genetically separable. Nucleic Acids Res *44*, 8241–8249.

Kagawa, W., Kurumizaka, H., Ishitani, R., Fukai, S., Nureki, O., Shibata, T., and Yokoyama, S. (2002). Crystal structure of the homologous-pairing domain from the human Rad52 recombinase in the undecameric form. Mol Cell *10*, 359–371.

Langerak, P., Mejia-Ramirez, E., Limbo, O., and Russell, P. (2011). Release of Ku and MRN from DNA ends by Mre11 nuclease activity and Ctp1 is required for homologous recombination repair of double-strand breaks. PLoS Genet *7*, e1002271.

Leland, B.A., and King, M.C. (2014). Using LacO arrays to monitor DNA double-strand break dynamics in live Schizosaccharomyces pombe cells. Methods Mol Biol *1176*, 127–141.

Lisby, M., Barlow, J.H., Burgess, R.C., and Rothstein, R. (2004). Choreography of the DNA damage response: spatiotemporal relationships among checkpoint and repair proteins. Cell *118*, 699–713.

Lord, C.J., Tutt, A.N.J., and Ashworth, A. (2015). Synthetic lethality and cancer therapy: lessons learned from the development of PARP inhibitors. Annu. Rev. Med. *66*, 455–470.

Ma, L., Milman, N., Nambiar, M., and Smith, G.R. (2015). Two separable functions of Ctp1 in the early steps of meiotic DNA double-strand break repair. Nucleic Acids Res *43*, 7349–7359.

Mateo, J., Carreira, S., Sandhu, S., Miranda, S., Mossop, H., Perez-Lopez, R., Nava Rodrigues, D., Robinson, D., Omlin, A., Tunariu, N., et al. (2015). DNA-Repair Defects and Olaparib in Metastatic Prostate Cancer. N. Engl. J. Med. *373*, 1697–1708.

Mimitou, E.P., and Symington, L.S. (2008). Sae2, Exo1 and Sgs1 collaborate in DNA double-strand break processing. *455*, 770–774.

Moreno, S., Klar, A., and Nurse, P. (1991). Molecular genetic analysis of fission yeast Schizosaccharomyces pombe. Meth. Enzymol. *194*, 795–823.

Nimonkar, A.V., Genschel, J., Kinoshita, E., Polaczek, P., Campbell, J.L., Wyman, C., Modrich, P., and Kowalczykowski, S.C. (2011). BLM-DNA2-RPA-MRN and EXO1-BLM-RPA-MRN constitute two DNA end resection machineries for human DNA break repair. Genes Dev *25*, 350–362.

Niu, H., Chung, W.-H., Zhu, Z., Kwon, Y., Zhao, W., Chi, P., Prakash, R., Seong, C., Liu, D., Lu, L., et al. (2010). Mechanism of the ATP-dependent DNA end-resection machinery from Saccharomyces cerevisiae. *467*, 108–111.

Ochs, F., Somyajit, K., Altmeyer, M., Rask, M.-B., Lukas, J., and Lukas, C. (2016). 53BP1 fosters fidelity of homology-directed DNA repair. Nat Struct Mol Biol *23*, 714–721.

Polato, F., Callén, E., Wong, N., Faryabi, R., Bunting, S., Chen, H.-T., Kozak, M., Kruhlak, M.J., Reczek, C.R., Lee, W.-H., et al. (2014). CtIP-mediated resection is essential for viability and can operate independently of BRCA1. J. Exp. Med. *211*, 1027–1036.

Rohner, S., Gasser, S.M., and Meister, P. (2008). Modules for cloning-free chromatin tagging in Saccharomyces cerevisae. Yeast *25*, 235–239.

Rosenberg, S.C., and Corbett, K.D. (2015). The multifaceted roles of the HORMA domain in cellular signaling. J Cell Biol *211*, 745–755.

Saad, H., Gallardo, F., Dalvai, M., Tanguy-le-Gac, N., Lane, D., and Bystricky, K. (2014). DNA dynamics during early double-strand break processing revealed by non-intrusive imaging of living cells. PLoS Genet *10*, e1004187.

Singleton, M.R., Wentzell, L.M., Liu, Y., West, S.C., and Wigley, D.B. (2002). Structure of the single-strand annealing domain of human RAD52 protein. Proc Natl Acad Sci USA *99*, 13492–13497.

Swartz, R.K., Rodriguez, E.C., and King, M.C. (2014). A role for nuclear envelope-bridging complexes in homology-directed repair. Mol Biol Cell *25*, 2461–2471.

Symington, L.S. (2016). Mechanism and regulation of DNA end resection in eukaryotes. Crit. Rev. Biochem. Mol. Biol. *51*, 195–212.

Symington, L.S., and Gautier, J. (2011). Double-strand break end resection and repair pathway choice. Annu Rev Genet *45*, 247–271.

Tkáč, J., Xu, G., Adhikary, H., Young, J.T.F., Gallo, D., Escribano-Díaz, C., Krietsch, J., Orthwein, A., Munro, M., Sol, W., et al. (2016). HELB Is a Feedback Inhibitor of DNA End Resection. Mol Cell *61*, 405–418.

Tomimatsu, N., Mukherjee, B., Deland, K., Kurimasa, A., Bolderson, E., Khanna, K.K., and Burma, S. (2012). Exo1 plays a major role in DNA end resection in humans and influences double-strand break repair and damage signaling decisions. DNA Repair (Amst.) *11*, 441–448.

Watson, A.T., Garcia, V., Bone, N., Carr, A.M., and Armstrong, J. (2008). Gene tagging and gene replacement using recombinase-mediated cassette exchange in Schizosaccharomyces pombe. Gene *407*, 63–74.

Watson, A.T., Werler, P., and Carr, A.M. (2011). Regulation of gene expression at the fission yeast Schizosaccharomyces pombe urg1 locus. Gene *484*, 75–85.

Watt, S., Mata, J., López-Maury, L., Marguerat, S., Burns, G., and Bähler, J. (2008). urg1: a uracil-regulatable promoter system for fission yeast with short induction and repression times. PLoS ONE *3*, e1428.

Wu, J.-Q., and Pollard, T.D. (2005). Counting cytokinesis proteins globally and locally in fission yeast. Science *310*, 310–314.

Xu, G., Chapman, J.R., Brandsma, I., Yuan, J., Mistrik, M., Bouwman, P., Bartkova, J., Gogola, E., Warmerdam, D., Barazas, M., et al. (2015). REV7 counteracts DNA double-strand break resection and affects PARP inhibition. Nature *521*, 541–544.

Yazinski, S.A., Comaills, V., Buisson, R., Genois, M.-M., Nguyen, H.D., Ho, C.K., Todorova Kwan, T., Morris, R., Lauffer, S., Nussenzweig, A., et al. (2017). ATR inhibition disrupts rewired homologous recombination and fork protection pathways in PARP inhibitor-resistant BRCA-deficient cancer cells. Genes Dev *31*, 318–332.

Zhu, Z., Chung, W.-H., Shim, E.Y., Lee, S.E., and Ira, G. (2008). Sgs1 helicase and two nucleases Dna2 and Exo1 resect DNA double-strand break ends. Cell *134*, 981–994.

Zimmermann, M., Lottersberger, F., Buonomo, S.B., Sfeir, A., and de Lange, T. (2013). 53BP1 regulates DSB repair using Rif1 to control 5' end resection. Science *339*, 700–704.

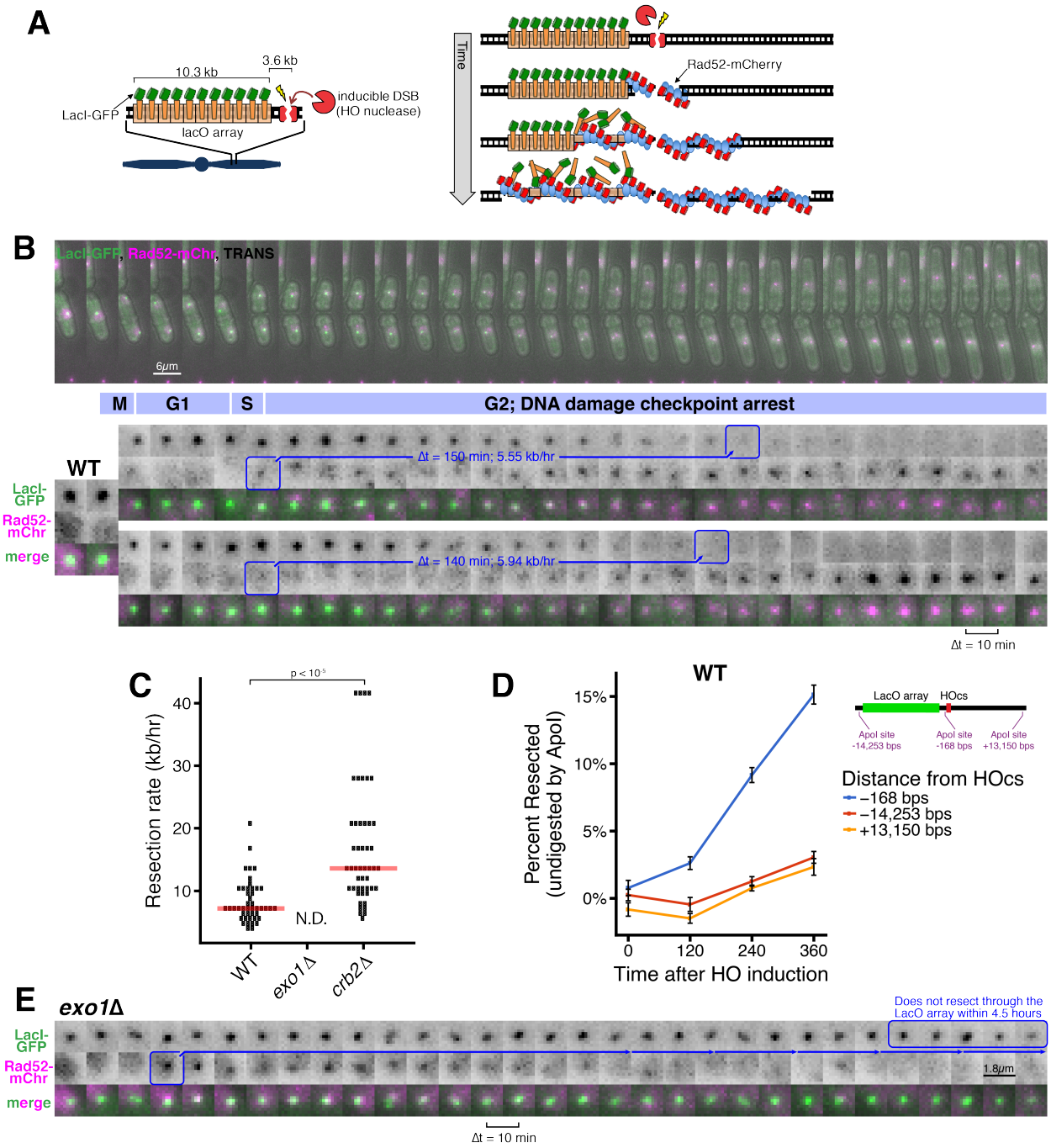

Figure 1. A microscopy-based assay to measure long-range resection in single cells.

(A) Design of the LacO resection assay in *S. pombe*. HO endonuclease cut cite (HOcs) and LacO integration at the *Mmf1* locus on Chr II allows live-cell measurements of resection rates. Rad52-mCherry loads on DSB ends after resection initiation, and LacI-GFP is displaced as resection creates long tracts of ssDNA through the LacO array.
(B) DSB resection events in two WT daughter cells. The majority of the *S. pombe* cell cycle is spent in G2, and all DSBs are observed in S/G2 based on the timing of mitosis and cell fission. Images shown are maximum intensity Z-projections acquired at 10-

minute time intervals. Blue annotations denote the starting point of resection (first frame with a detectable Rad52 focus, which formation shortly after resection begins) and the end point (first frame with total loss of the LacO/LacI-GFP focus) of individual resection events. These start/end frames mark the total duration of resection through the 13.87 kb distance between the HOcs and the distal end of the repetitive LacO array, and are used to compute resection rate (kb/hr) for individual cells.
(C) Single-cell measurements of resection rate using the LacO resection assay. Horizontal red bars mark the median resection rate for each genotype. *exo1*Δ rates cannot be determined (N.D.) because resection through the LacO array does not complete within 5 hrs of data acquisition. p-values shown are from pairwise two-tailed t-tests, using a Bonferroni correction for multiple comparisons. Number of biological replicates and counts of analyzed cells can be found in Supplementary file 2.
(D) The rate of resection is equivalent on both the LacO and non-LacO sides of the HOcs in WT cells. Average long-range resection at the population level assessed by an orthogonal qPCR assay that quantifies the percentage of chromosomes that have undergone resection through ApoI sites at various distances from the HOcs. Resection to single-stranded DNA through an ApoI site protects that site from digestion by the double-strand specific nuclease, ApoI. Error bars show 95% CIs for three technical qPCR replicates.
(E) Representative resection-deficient *exo1*Δ cell that that loads on-target Rad52-mCherry but does not lose the LacO/LacI-GFP focus. Because resection of the LacO array is too slow to be completed during the window of data acquisition, we are not able to quantify the rate of resection in *exo1*Δ cells.

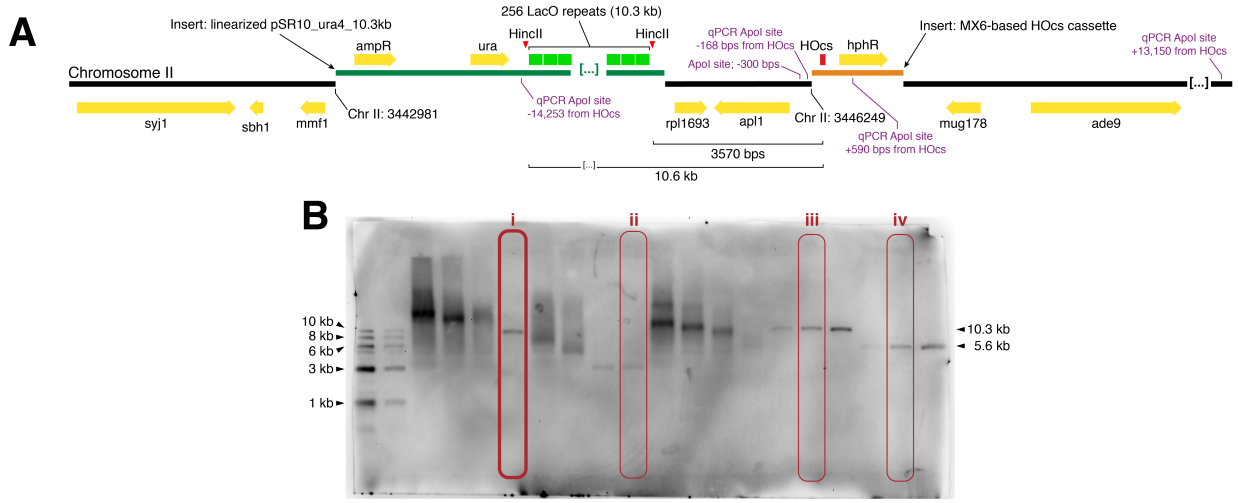

Figure 1–figure supplement 1.
(A) Map of LacO array integration and HO cut cite integration in *S. pombe* (Chr II: 3,442,981 and Chr II: 3,446,249, respectively) drawn to scale (note: only 6 of the ~256 LacO repeats are shown).
(B) Verification of LacO array length after integration into *S. pombe* by HincII digest and Southern blot with a LacO-targeted probe. Circled lanes: (i) MKSP1381: the *S. pombe* strain with a complete 10.3 kb LacO array integration used to derive all LacO assay strains used in this study; (ii) MKSP1173: a strain where the LacO array contracted upon integration to < 5 kb (not used for LacO resection assay); (iii) pSR10_ura4_10.3kb and (iv) pSR10_ura4_5.6kb are plasmids with LacO arrays of known size. Linearized pSR10_ura4_10.3kb was integrated into *S. pombe*.

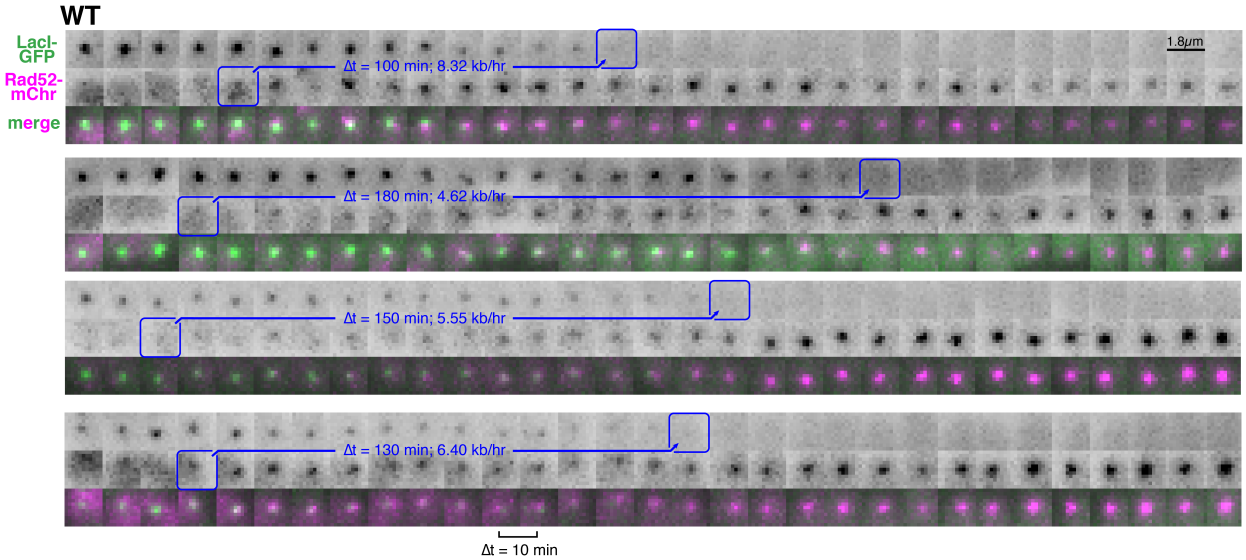

Figure 1–figure supplement 2.
Additional examples of the LacO resection assay in individual WT cells. As in Figure 1, the blue annotations denote the starting point of resection (first frame with a detectable Rad52 focus, which formation shortly after resection begins) and the end point (first frame with total loss of the LacO/LacI-GFP focus) of individual resection events. These start/end frames mark the total duration of resection through the 13.87 kb distance between the HOcs and the distal end of the repetitive LacO array, and are used to compute resection rate (kb/hr) for individual cells.

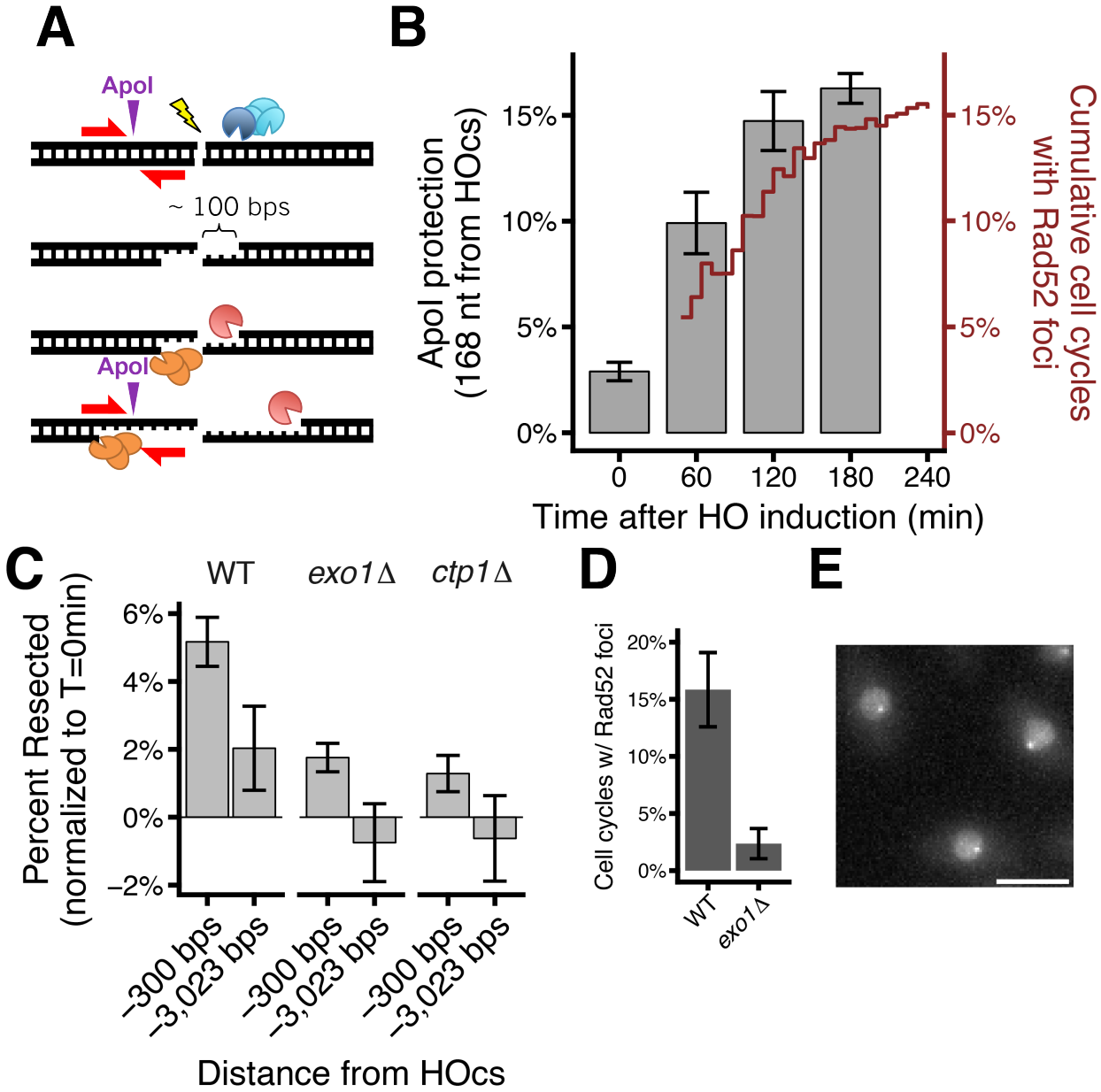

Figure 1–figure supplement 3.

(A) Diagram of the qPCR assay. Resection at the HO-induced DSB generates ssDNA through the ApoI site 168 nt from the HO cut cite, protecting from ApoI digestion.

(B) Kinetics of resection assessed by qPCR and Rad52 loading. Percentage of chromosomes that have undergone 168 nt of resection at the HO cut cite over time, measured by the ApoI-site protection-based qPCR assay (bars, left y-axis). Error bars show SEM for three technical qPCR replicates. Corresponding data for Rad52-mCherry focus formation in the LacO resection assay (red line, right y-axis).

(C) Resection rates, measured by a population-based qPCR assay, at various distances from the HOcs in *exo1*Δ and *ctp1*Δ cells. Resection to single-stranded DNA through an ApoI site at the indicated positions relative to the HO cut site protects that site from

digestion by the double-strand specific nuclease, ApoI. Error bars show 95% CIs for three technical qPCR replicates.

(D) On-target Rad52-mCherry foci form at reduced rates in *exo1*Δ cells. p-value shown is from pairwise two-tailed t-tests, using a Bonferroni correction for multiple comparisons. Number of biological replicates and counts of analyzed cells can be found in Supplementary file 2.

(E) Represent micrograph of a strain expressing GFP-LacI with an integrated 1 kb LacO array under the imaging conditions used in the assay (Figure 1). Based on the robustness of this signal, we estimate that the threshold of detection in the assay is <500 bp of LacO array (half the signal to noise in this image). Scale bar = 5 μm

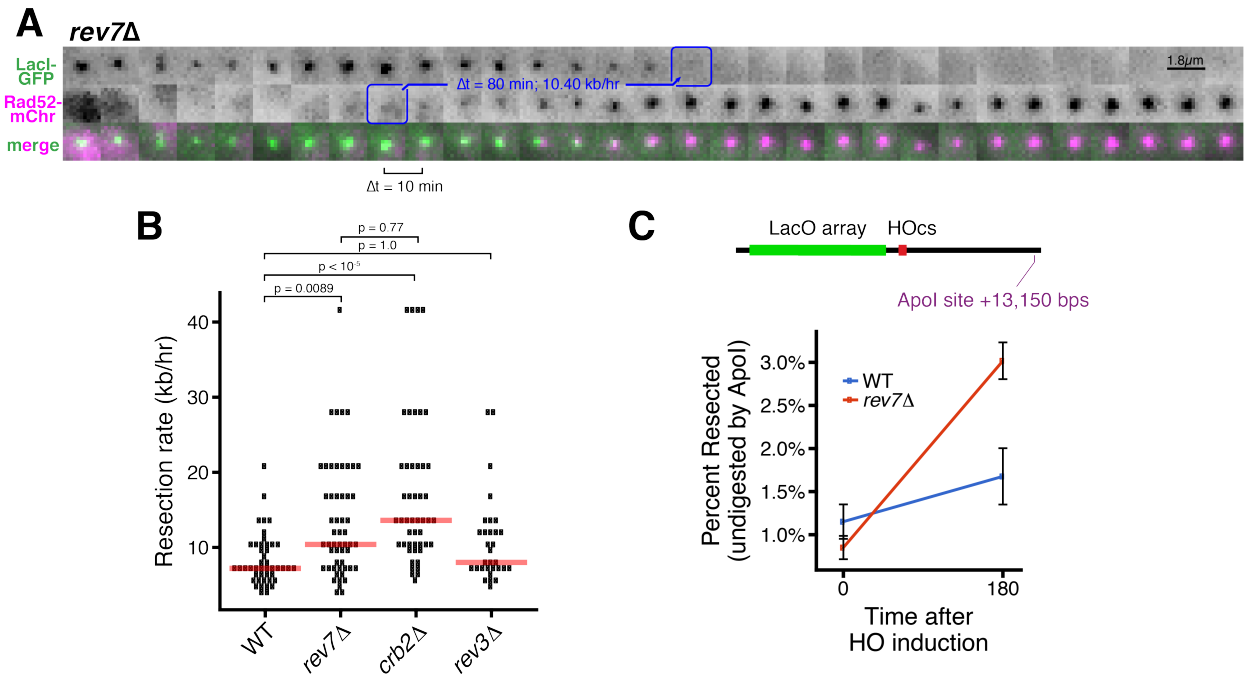

Figure 2. Loss of Rev7 causes an increase in long-rage resection comparable to the loss of Crb2.

(A) Representative timeseries of a resection through the LacO array in a single *rev7*Δ cell. Blue annotations mark the beginning and end of individual resection events, as in Figure 1B.

(B) Single-cell measurements of resection rate using the LacO resection assay. Horizontal red bars mark the median resection rate for each genotype. p-values shown are from pairwise two-tailed t-tests, using a Bonferroni correction for multiple comparisons. Number of biological replicates and counts of analyzed cells can be found in Supplementary file 2.

(C) The long-range rate of resection *rev7*Δ and WT, measured with an ApoI protection qPCR assay on a population level on the side. The ApoI cut site used here is on opposite side of HOcs from the LacO array. Error bars show 95% CIs for three technical qPCR replicates.

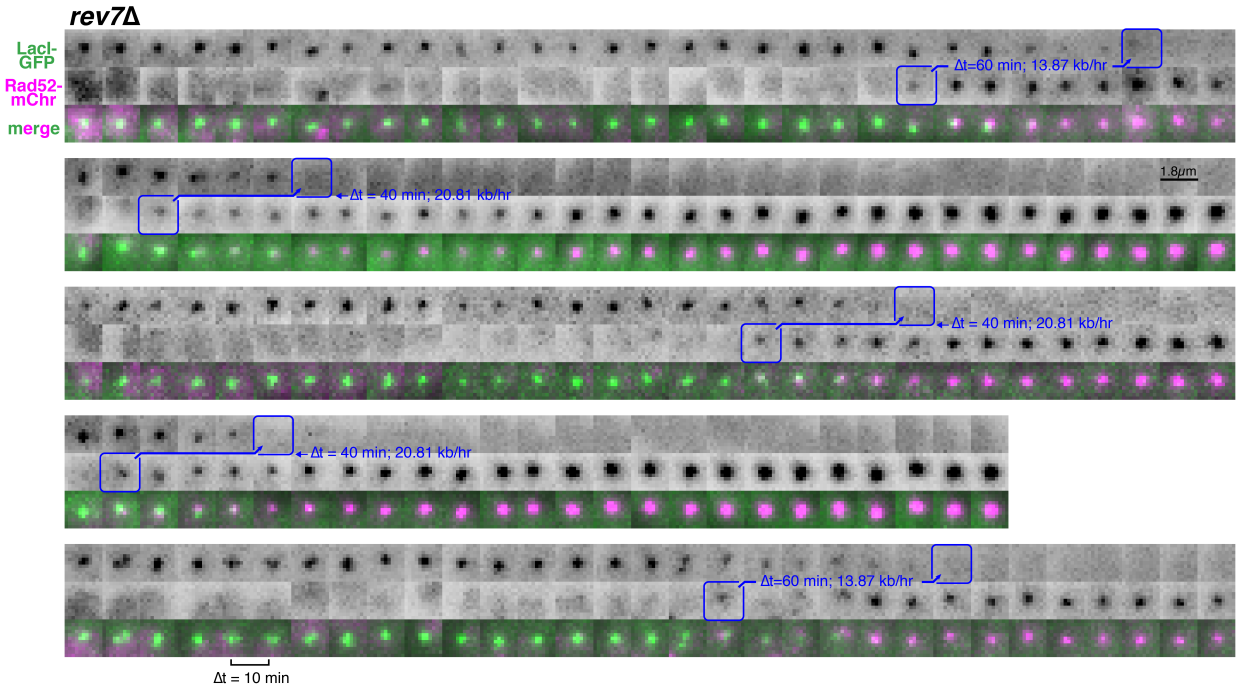

Figure 2–figure supplement 1.
Additional examples of rapid long-range resection through the LacO array in *rev7*Δ cells. Blue annotations mark the beginning and end of individual resection events, as in Figure 1B.

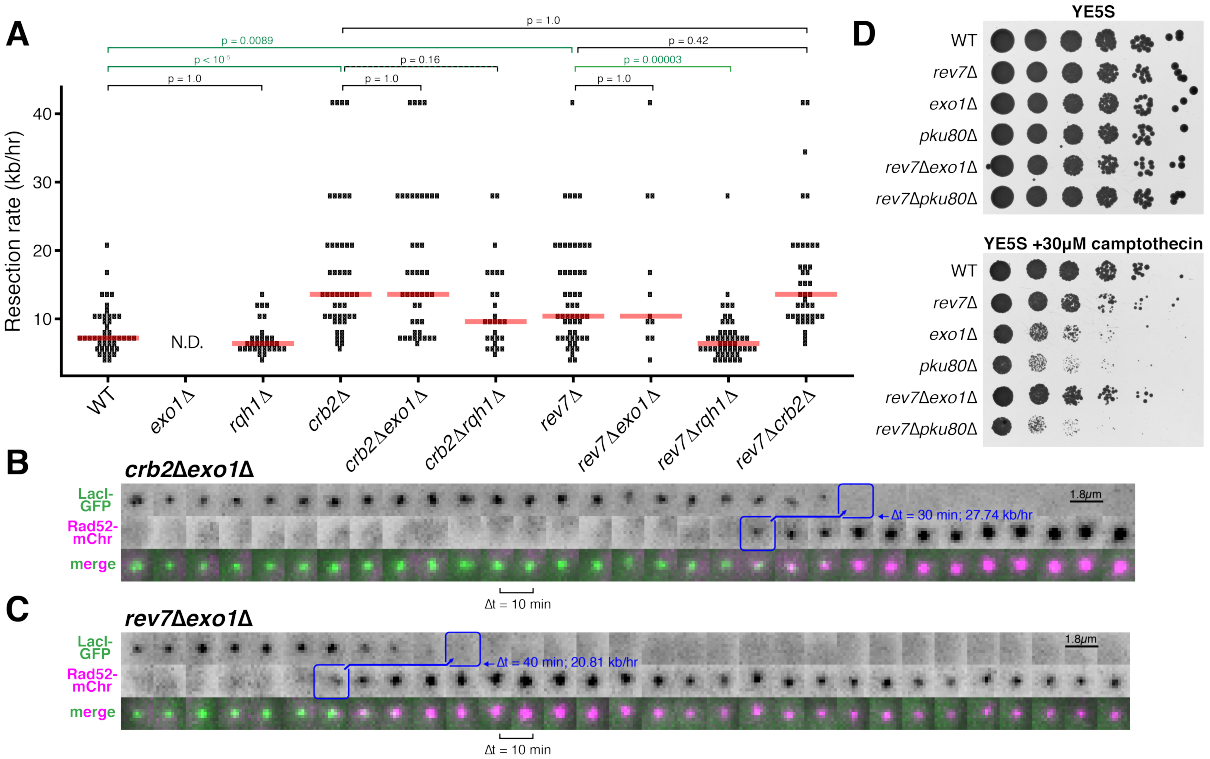

Figure 3. Rev7 and Crb2 act through the RecQ helicase, Rqh1, and not Exo1, to inhibit long-range resection.

(A) Epistasis analysis of long-range resection rates from single-cell measurements. *exo1*Δ rates cannot be determined (N.D.) because resection through the LacO array does not complete within 5 hrs of data acquisition. Red bars show median resection rates and p-values are from pairwise two-tailed t-tests, using a Bonferroni correction for multiple comparisons (significant comparisons shown in green; see text).

(B,C) Very rapid resection through the 10.3 kb LacO array is common in *crb2*Δ*exo1*Δ (B) and *rev7*Δ*exo*Δ (C) cells, in contrast to *exo1*Δ single mutants that do not completely resect the LacO array within 5 hrs (see Figure 1D). (D) Growth assay on rich media with and without camptothecin. Loss of Rev7 can rescue the severe growth defect of *exo1*Δ cells.

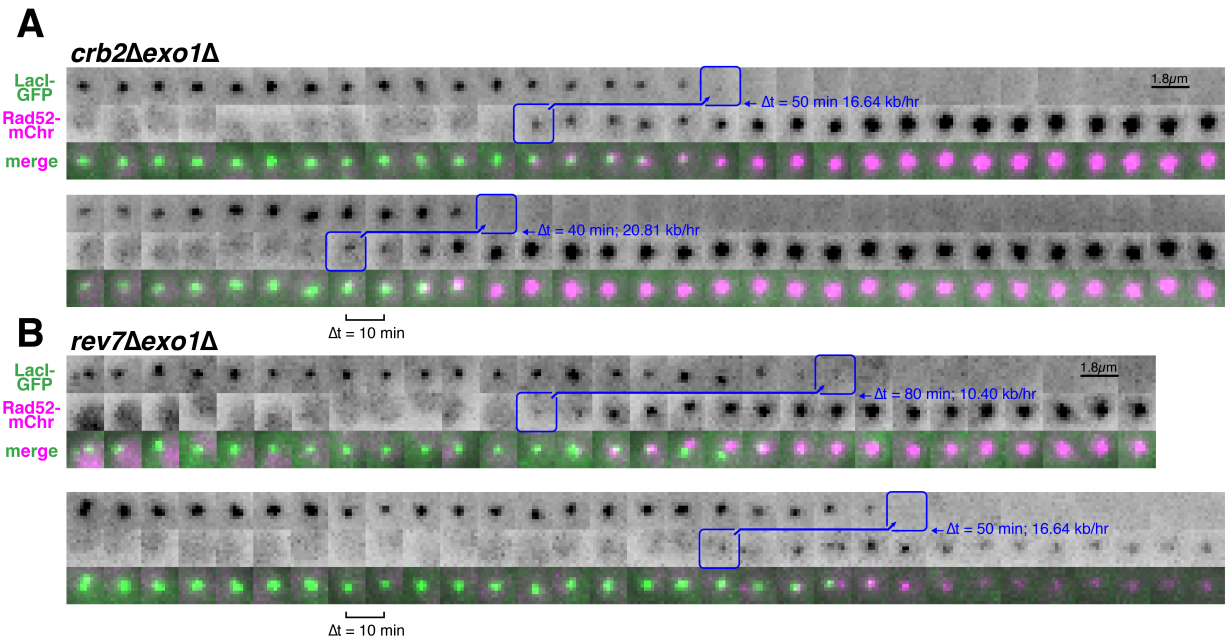

Figure 3–figure supplement 1.
Additional examples of very rapid resection through the LacO array in individual *crb2Δexo1Δ* (A) and *rev7Δexo*Δ (B) cells.

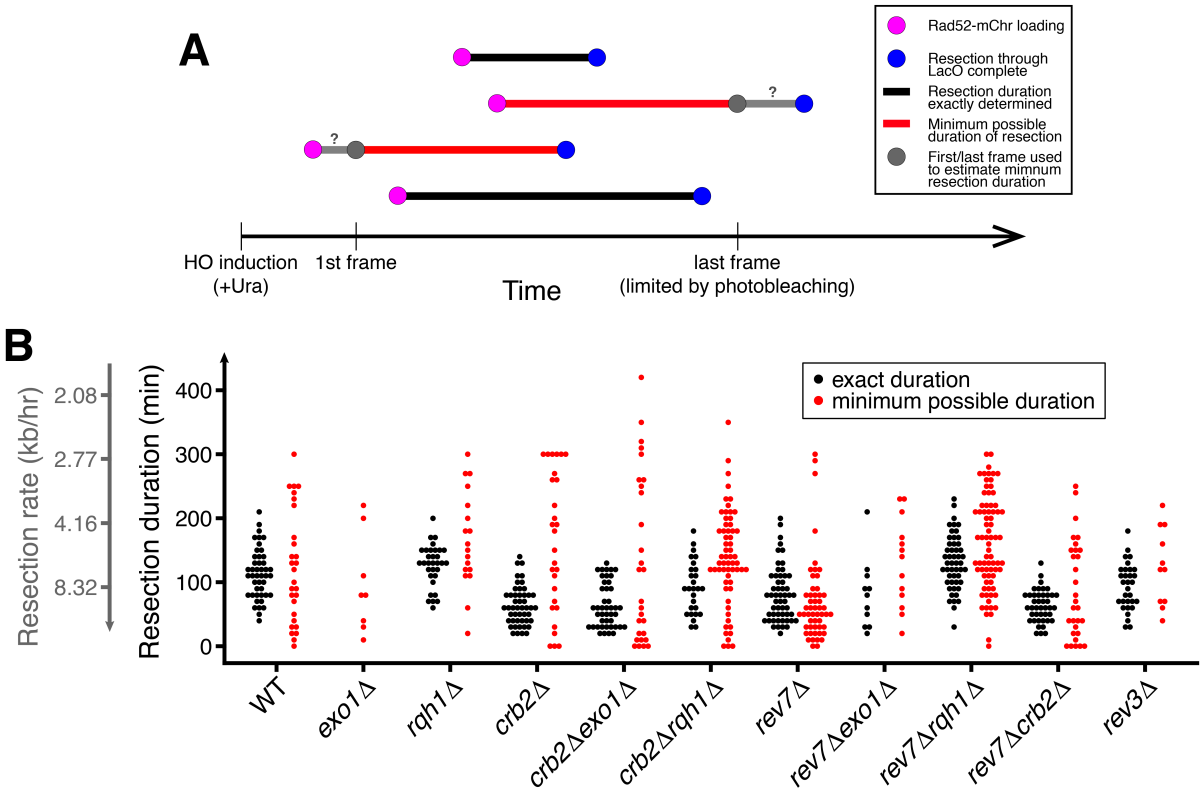

Figure 3–figure supplement 2.
(A) Diagram of exactly and non-exactly determined resection events. The LacO resection assay is limited to 5 hrs due to photobleaching. Thus, many resection events will start before the first frame or end after the last frame of data acquisition (red). Longer durations (slower resection) are more likely to extend past the first or last frame, and the lower threshold for exactly determined resection rates is 2.8 kb/hr for 5 hrs of data acquisition.
(B) Duration of individual resection events through the 10.3 kb LacO array (secondary y-axis shows resection rate). Minimum possible durations are shown in red. Of particular note, many slow *crb2*Δ*rqh1*Δ events have longer durations (slower rates) and thus they cannot be exactly determined. See Supplementary file 2 for number of biological replicates and counts of analyzed cells.

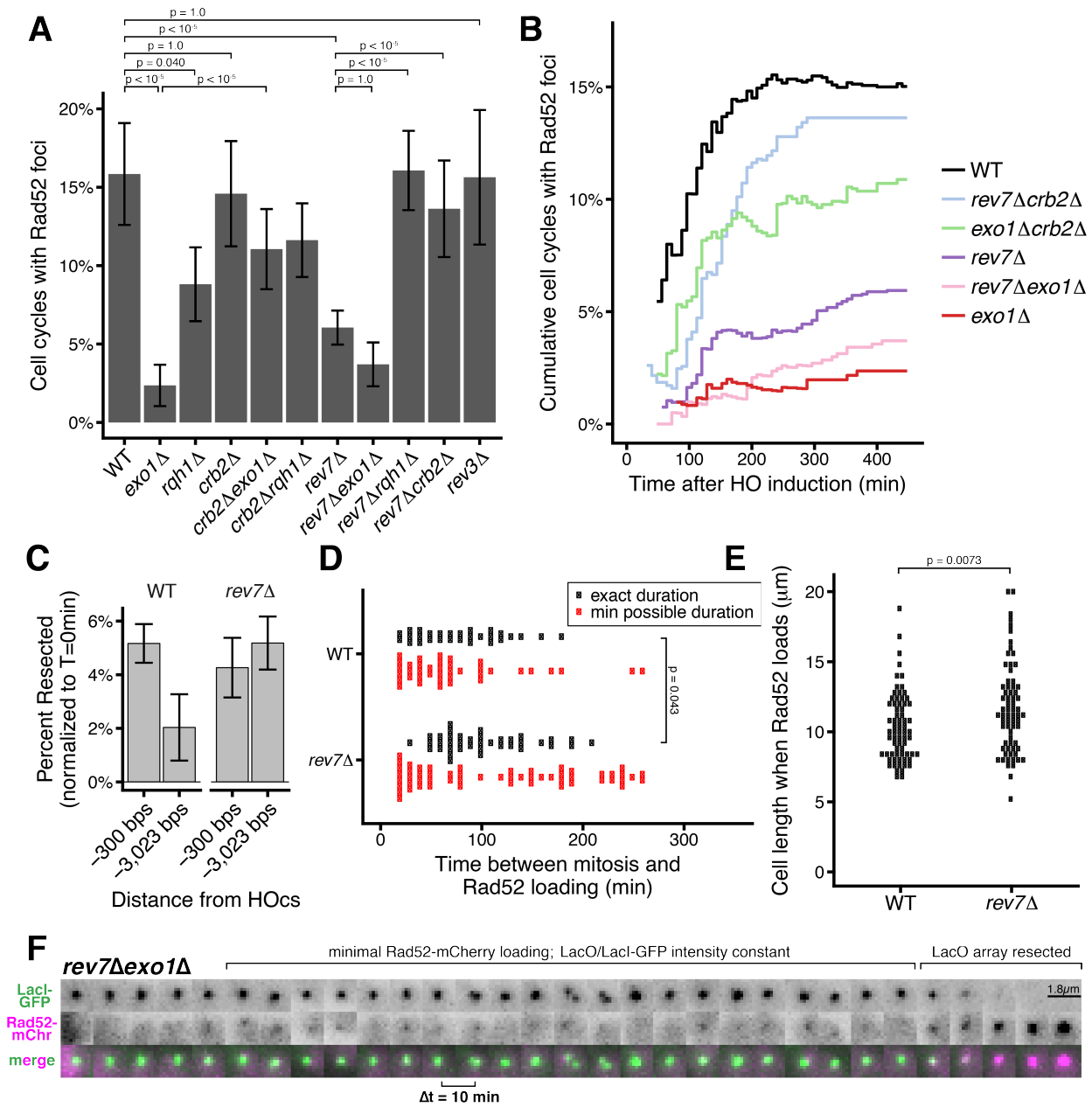

Figure 4. Rev7, unlike Crb2, promotes DSB proximal resection.

(A) Percentage of observed cell cycles in which an on-target Rad52-focus formed during the 5 hrs of data acquisition. Error bars show binomial proportion 95% CIs, p-values are from pairwise two-tailed proportion tests, using a Bonferroni correction for multiple comparisons.

(B) Timing of on-target Rad52 loading events. Time after HO endonuclease induction was binned into 8-minute intervals, and the cumulative number of cell cycles and on-target Rad52 loading events were counted in each interval.

(C) The extent of resection 300 bps and 3 kb from the HO cut site as assessed by the restriction enzyme/qPCR method supports less efficient resection initiation in *rev7*Δ cells compared to WT at 300 bp, while *rev7*Δ cells show a gain of resection efficiency 3 kb

away from the HO cut site, consistent with more rapid long-range resection (Figure 1). Resection to single-stranded DNA through the ApoI site at the indicated distances from the HO cut site protects that site from digestion by the double-strand specific nuclease, ApoI. Error bars show 95% CIs for three technical qPCR replicates.
(D) Delay between mitosis (nuclear division) and on-target Rad52 loading events in individual *rev7*Δ cells. Events in which the nuclear division happens before the first frame of data acquisition cannot be exactly determined, so minimum possible durations are shown in red. p-value is from a two-tailed t-test on exactly determined durations (black).
(E) Cell length (a proxy for cell cycle checkpoint arrest in *S. pombe*) at the time of on-target Rad52 focus formation. p-value is from a two-tailed t-test.
(F) An example of low-levels of Rad52 persisting at the DSB for > 2 hours, barely above the limits of detection. Then rapid, processive, long-range resection through the LacO array occurs. See Supplementary file 2 for number of biological replicates and counts of analyzed cells pertaining to (A-B, D-E).

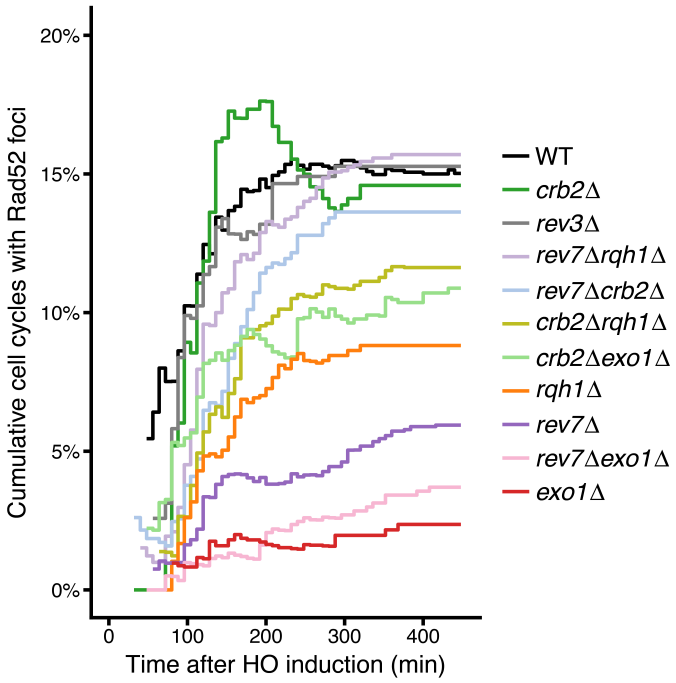

Figure 4–figure supplement 1.
Timing of on-target Rad52 loading events, as in Figure 4B, for all genotypes. See Supplementary file 2 for number of biological replicates and counts of analyzed cells.

Supplementary file S1: Strains used in this study. These strains were for all LacO resection assay experiments in Figures 1-4 unless otherwise noted. P_{Dis1}-GFP-LacI-NLS is derived from Shimada et al. 2003. LacO integrations were performed as described in Leland and King, 2014. Strains containing the RMCE $P_{urg1lox}$ expression system were derived from Watson et al., 2011.

References:

Leland, B.A., and King, M.C. (2014). Using LacO arrays to monitor DNA double-strand break dynamics in live Schizosaccharomyces pombe cells. Methods Mol Biol *1176*, 127–141.

Shimada, T., Yamashita, A., and Yamamoto, M. (2003). The fission yeast meiotic regulator Mei2p forms a dot structure in the horse-tail nucleus in association with the sme2 locus on chromosome II. Mol Biol Cell *14*, 2461–2469.

Watson, A.T., Werler, P., and Carr, A.M. (2011). Regulation of gene expression at the fission yeast Schizosaccharomyces pombe urg1 locus. Gene *484*, 75–85.

Strain	Description	Complete Genotype
MKSP1381	Original LacO integration used to generate all other strains in this study (Figure S1B)	*h- leu1-32 ura4-D18 his7+:P_{Dis1}-GFP-LacI-NLS ChrII:3442981::Ura4-10.3kbLacO ChrII:3446249::HOcs-hphMX6 Cut11-mCherry::natMX6*
MKSP1173	Example of LacO array contracting upon integration (Figure S1B)	*h- leu1-32 ura4-D18 his7+:P_{Dis1}-GFP-LacI-NLS Leu2::Ura4-LacO<5kb Rad26-mCherry::natMX6*
MKSP2123	WT LacO resection assay	*h- leu1-32 ura4-D18 his7+:P_{Dis1}-GFP-LacI-NLS ChrII:3442981::Ura4-10.3kbLacO ChrII:3446249::HOcs-bleMX6 Rad52-mCherry::bleMX6 urg1::RMCE-bleMX6*
MKSP1914	*exo1*Δ LacO resection assay	*h- leu1-32 ura4-D18 his7+:P_{Dis1}-GFP-LacI-NLS ChrII:3442981::Ura4-10.3kbLacO ChrII:3446249::HOcs-hphMX6 Rad52-mCherry::natMX6 urg1::RMCE-kanMX6 exo1::bleMX6*
MKSP2501	*rqh1*Δ LacO resection assay	*h- leu1-32 ura4-D18 his7+:P_{Dis1}-GFP-LacI-NLS ChrII:3442981::Ura4-10.3kbLacO ChrII:3446249::HOcs-hphMX6 Rad52-mCherry::bleMX6 urg1::RMCE-bleMX6 rqh1::kanMX6*
MKSP2244	*crb2*Δ LacO resection assay	*h- leu1-32 ura4-D18 his7+:P_{Dis1}-GFP-LacI-NLS ChrII:3442981::Ura4-10.3kbLacO ChrII:3446249::HOcs-hphMX6 Rad52-mCherry::bleMX6 urg1::RMCE-bleMX6 crb2::kanMX6*

MKSP2476	*crb2*Δ*exo1*Δ LacO resection assay	*h+ leu1-32 ura4-D18 his7+:*P_{Dis1}*-GFP-LacI-NLS ChrII:3442981::Ura4-10.3kbLacO ChrII:3446249::HOcs-hphMX6 Rad52-mCherry::bleMX6 urg1::RMCE-bleMX6 crb2::kanMX6 exo1::bleMX6*
MKSP2479	*crb2*Δ*rqh1*Δ LacO resection assay	*h+ leu1-32 ura4-D18 his7+:*P_{Dis1}*-GFP-LacI-NLS ChrII:3442981::Ura4-10.3kbLacO ChrII:3446249::HOcs-hphMX6 Rad52-mCherry::bleMX6 urg1::RMCE-bleMX6 crb2::kanMX6 rqh1::kanMX6*
MKSP2149	*rev7*Δ LacO resection assay	*h+ leu1-32 ura4-D18 his7+:*P_{Dis1}*-GFP-LacI-NLS ChrII:3442981::Ura4-10.3kbLacO ChrII:3446249::HOcs-hphMX6 Rad52-mCherry::bleMX6 urg1::RMCE-bleMX6 rev7::natMX6*
MKSP2392	*rev7*Δ*exo1*Δ LacO resection assay	*h+ leu1-32 ura4-D18 his7+:*P_{Dis1}*-GFP-LacI-NLS ChrII:3442981::Ura4-10.3kbLacO ChrII:3446249::HOcs-hphMX6 Rad52-mCherry::bleMX6 urg1::RMCE-bleMX6 rev7::natMX6 exo1::bleMX6*
MKSP2456	*rev7*Δ*rqh1*Δ LacO resection assay	*h+ leu1-32 ura4-D18 his7+:*P_{Dis1}*-GFP-LacI-NLS ChrII:3442981::Ura4-10.3kbLacO ChrII:3446249::HOcs-hphMX6 Rad52-mCherry::bleMX6 urg1::RMCE-bleMX6 rev7::natMX6 rqh1::kanMX6*
MKSP2245	*rev7*Δ*crb2*Δ LacO resection assay	*h+ leu1-32 ura4-D18 his7+:*P_{Dis1}*-GFP-LacI-NLS ChrII:3442981::Ura4-10.3kbLacO ChrII:3446249::HOcs-hphMX6 Rad52-mCherry::bleMX6 urg1::RMCE-bleMX6 rev7::natMX6 crb2::kanMX6*
MKSP2262	*rev3*Δ LacO resection assay	*h+ leu1-32 ura4-D18 his7+:*P_{Dis1}*-GFP-LacI-NLS ChrII:3442981::Ura4-10.3kbLacO ChrII:3446249::HOcs-hphMX6 Rad52-mCherry::bleMX6 urg1::RMCE-bleMX6 rev3::kanMX6*
MKSP2477	*ctp1*Δ LacO resection assay	*h+ leu1-32 ura4-D18 his7+:*P_{Dis1}*-GFP-LacI-NLS ChrII:3442981::Ura4-10.3kbLacO ChrII:3446249::HOcs-hphMX6 Rad52-mCherry::bleMX6 urg1::RMCE-bleMX6 ctp1::kanMX6*

Supplementary file S2: Number of biological replicates, cell cycles, and DSB events analyzed for each genotype. These counts pertain to all data from the resection assay in Figures 1-4.

Genotype	Number of biological replicates	Total cell cycles observed	Number of dead or sick cells*‡	Number of daughter cell cycles whose parent had an on-target DSB*‡	Number of cell cycles observed for < 100 minutes prior to photobleaching of the field‡	Observed cell cycles valid for %Rad52 calculations	Number of Rad52 focus formation events	Number of resection events that are exactly determined
WT	6	1049	27	52	484	486	77	45
*exo1*Δ	4	945	13	2	422	508	8	0
*rqh1*Δ	6	991	61	2	372	556	49	32
*crb2*Δ	5	1045	78	164	378	425	62	48
*crb2*Δ*exo1*Δ	4	1122	42	128	373	579	64	44
*crb2*Δ*rqh1*Δ	3	1207	73	70	350	714	83	27
*rev7*Δ	5	3182	190	24	1117	1851	112	54
*rev7*Δ*exo1*Δ	8	1251	70	2	477	702	26	11
*rev7*Δ*rqh1*Δ	7	1311	57	10	435	809	130	50
*rev7*Δ*crb2*Δ	3	1122	43	88	514	477	65	42
*rev3*Δ	2	637	21	24	317	275	43	31

* Cell cycles that were excluded from the analyses of resection rate in Figures 1C, 2B, 3A

‡ Cell cycles that were excluded from %Rad52 calculations in Figures 1-S3B, 1-S3D, 4A, 4B, 4-S1

Supplementary file S3. Primers sets used in qPCR measurements of resection.

ApoI site position relative to HOcs at Mmf1	Forward primer	Reverse primer
-168v1	ATCACCGATGGAAACAGTGAACTCAT	GCTGATTTGCTAGCAGTCTTCAGCTC
-168v2	GGAAACAGTGAACTCATATCATATCCA	GCAGTCTTCAGCTCAGATAATAAGG
-300	AGAAACTTTTACAAACCTCGCGT	TGAGTTCACTGTTTCCATCGGT
-3023	AGCTTGTAATAATCGATGCCAAAGG	GTTGAGGCTAAACGACCCATT
+13150	GCCAGCTATGACAAAAGGCC	TAGGATCGTAGTTGCCAGCG
-14253	AGCTGGTTGGAAGGCATATCA	CGCAAACAAGGCATCGACTTT
Control primers		
Ncb1v0	AGACGTATTTGAGTGATAGTGCTCGCTGC	CGTCCTTCCGATGTTGCTTTAACGCATACTC
Ncb1v1	GCCGCTGAACACATTATTAAAGC	CGCCACTTCCAAAGCTTCAG

The -168v1 and Ncb1v0 primers were used in panel Figure 1 – figure supplement 3B. For all other plots, the -168v2 and Ncb1v1 primers were used.